The Side Plume of Magnetically Shielded Hall Thrusters

IEPC-2022-402

Presented at the 37th International Electric Propulsion Conference
Massachusetts Institute of Technology, Cambridge, MA USA
June 19-23, 2022

Wensheng Huang[1] and Hani Kamhawi[2]
National Aeronautics and Space Administration Glenn Research Center, Cleveland, OH, 44135, USA

A combination of near-thruster laser-induced fluorescence and far-field plasma probe measurements collected from two magnetically shielded Hall thrusters have shown that there exist an independent ion population of medium-energy (on average, 60-190 eV) exiting out the side (60° to 100° from firing axis) of the thrusters. Studying the trends with background pressure and known discrepancies between the laser-induced fluorescence and far-field plasma probe data suggest that at zero pressure the side plume is likely to exhibit higher energy and lower density than at facility background pressures. The possibility that these ions were produced by the modified two-stream instability is explored and while the agreement is good, there are areas of notable disagreement. Based on the idea that production of the side plume and channel exit striations are due to the same plasma wave actions, a theory was explored that explains why striations form under certain circumstances but not others. Another theory, based on the idea that side plume production only occurs over certain portion of the global discharge oscillation cycle, was also explored and areas of disagreement were identified. While the exact mechanism for side plume acceleration remains unclear, if the theory behind side plume production is correct, then side plume can be expected to be present in a wide range of magnetically-shielded as well as non-shielded Hall thrusters.

I. Introduction

Over the past decade of Hall thruster research, a body of evidence has surfaced that points to the existence of a mildly energetic (averaged energy of 60-190 eV), low-density ion population exiting the side (60-100° from firing axis) of magnetically-shielded Hall thrusters. Initially, this side plume was thought to be a result of charge-exchange actions in the thruster plume [1]. New data from laser-induced fluorescence tests show that the side plume is likely to be an ion population independent of both the main beam and the charge-exchange population and originates from the chamfer regions of the thruster discharge channel [2]. Known characteristics of this side plume will be examined and implications for future applications of Hall thrusters will be briefly discussed.

Section II of this paper will examine the collection of experimental data pointing to the existence of an independent side plume in magnetically-shielded Hall thrusters, with a focus on the Hall Effect Rocket with Magnetic Shielding (HERMeS) and its successor Advanced Electric Propulsion System (AEPS) Hall thrusters. Data examined will include near-field laser-induced fluorescence (LIF) velocimetry, far-field Faraday probe and retarding potential analyzer (RPA), and physical features that form from erosion. This section will also describe the known characteristics of the side plume. Section III of this paper will point out disagreements in the presented data and the likely explanation for the disagreement. Section IV will describe a few hypotheses on the nature of the side plume and areas of agreement and disagreement with the data. Section V briefly discuss the implications of the hypotheses for future thruster applications. Section VI will provide a brief summary of the preceding sections.

[1] Research Engineer, Electric Propulsion Systems Branch, AIAA Associate Fellow, wensheng.huang@nasa.gov.
[2] Research Engineer, Electric Propulsion Systems Branch, AIAA Associate Fellow, hani.kamhawi-1@nasa.gov.

II. The Evidence

For this paper, throttle points are labeled by discharge voltage and discharge power. A label that says "300-6.3-B1.00" refers to the throttle point with a discharge voltage of 300 V and a discharge power of 6.3 kW. The value after the letter B indicates multiple of nominal magnetic field strength. For example, "B1.25" indicates 1.25 times the nominal magnetic field strength. If no B value is shown, the B value is 1. Some labels include "VF5" for Vacuum Facility 5 and "VF6" for Vacuum Facility 6, both of which are located at the Glenn Research Center.

A. Laser-Induced Fluorescence Data

In 2018, a LIF test was performed on the HERMeS Technology Development Unit (TDU) in Vacuum Facility 6 [3]. This was followed by a LIF test on the AEPS Engineering Test Unit (ETU) in Vacuum Facility 5 [2]. Both thrusters are 12.5-kW magnetically-shielded thrusters with centrally mounted cathodes. In both tests, ions found near the outer front pole exhibited much higher energy (50-200 eV) than can be explained by charge-exchange actions. These ions were found, on average, to travel nearly parallel to the outer front pole. At locations near the chamfer these "medium-energy" ions were found to co-exist with the high-energy main beam ions. At these locations, the use of three laser axes made it possible to isolate each population and determine that the characteristics of one population match beam ions while the other match those found near the outer front pole [3]. Fig. 1 shows an example where the medium-energy population was found to co-exist with the high-energy main beam population. In subplot (a), main beam ions were plotted as black arrows and medium-energy ions were plotted as green arrows. Subplots (b), (c), (d) shows the LIF data and associated curve-fits from the marked location for three separate laser axes. Subplot (b) shows the axial laser axis results, (c) shows results of the side axis -45 degree from the firing axis, and (d) shows the results of the side axis +45 degree from the firing axis. In this figure, positive angle means the laser optics are located to the right of the firing axis and vice versa. This data shows that the medium-energy ions were clearly distinguishable from the main beam ions.

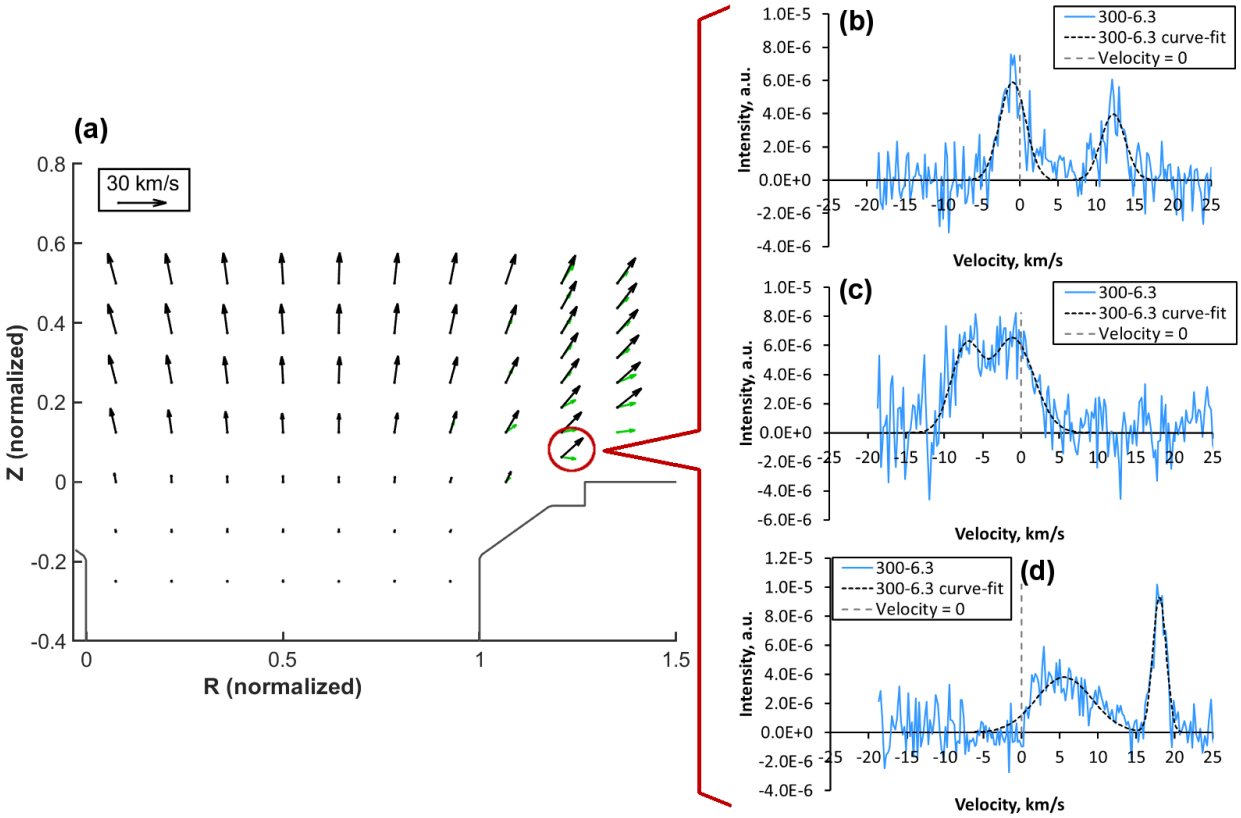

Fig. 1. Example LIF data showing that the medium-energy population and the high-energy beam population are separate ion populations. Subplot (a) shows the averaged ion vectors near the discharge channel where black arrows indicate main beam ions and green arrows indicate the medium-energy ions. Subplots (b), (c), (d) shows the LIF data and the associated curve-fits from the marked location for three separate laser axes.

Using the same Monte Carlo re-sampling method for constructing the ion energy distribution as described in reference [3], one can construct the ion angular distribution. Fig. 2 shows an example of this construction as applied to TDU data. Table 1 summarizes the basic statistical parameters derived from the energy and angle distribution for a number of TDU and ETU operating conditions at various background pressures. Each entry was obtained by averaging over all measurement locations near the outer front pole. See references [3] and [2] for data locations and test setup for the TDU test in VF6 and ETU test in VF5, respectively. In Table 1, the headings "E_{AVG}" and "E_{FWHM}" refer to the averaged energy and full-width-at-half-maximum energy, respectively, calculated from the energy distribution. "Avg. Angle" refers to the averaged angle calculated from the angle distribution. "90% bound" refers to the bounding angles between which 90% of the ions in the angle distribution lies. For angles reported in this paper, 0 degree correspond to pointing directly downstream, positive when pointing radially outward, and negative when pointing radially inward.

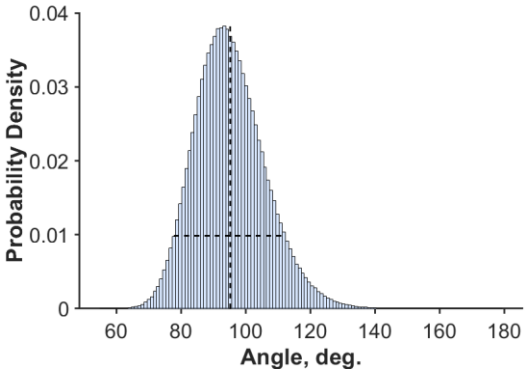

Fig. 2. An example of applying the Monte Carlo re-sampling method [3] to construct the ion angular distribution from two orthogonal axes of LIF data.

Table 1. TDU and ETU outer front pole energy and angle characteristics.

Thruster	Condition	Facility	Pressure, uT	Sample Size	E_{AVG}, eV	E_{FWHM}, eV	Avg. Angle, degree	90% bound, degree
TDU1	300-2.4	VF6	5	5	175	92	92	81-103
TDU1	300-2.4	VF6	10	5	171	98	90	78-102
TDU1	300-2.4	VF6	18	5	161	118	92	77-107
TDU1	300-2.4	VF6	27	5	132	119	93	69-117
TDU1	300-2.4	VF6	37	5	104	107	94	67-123
TDU1	300-6.3	VF6	12	8	119	77	96	82-110
TDU1	300-6.3	VF6	16	4	103	88	97	78-116
TDU1	300-6.3	VF6	22	4	112	78	98	81-115
TDU1	300-9.4	VF6	16	5	98	91	100	78-121
TDU1	400-8.3	VF6	12	2	101	108	98	67-129
TDU1	400-12.5	VF6	16	2	112	95	101	73-128
TDU1	500-10.4	VF6	12	3	100	101	92	63-121
TDU1	600-12.5	VF6	12	1	101	105	105	81-128
TDU1	600-12.5	VF6	22	2	63	70	109	89-141
ETU2	300-3	VF5	2.7	7	164	78	96	85-106
ETU2	300-4.5	VF5	3.9	6	121	79	96	82-110
ETU2	300-6.3	VF5	5	11	119	90	100	81-118
ETU2	300-6.3	VF5	12	5	108	86	101	81-121
ETU2	400-8.3	VF5	5	3	127	99	105	78-132
ETU2	500-10.4	VF5	5	1	90	92	98	76-121
ETU2	600-12.5	VF5	5	1	121	67	90	78-102
ETU2	600-12.5	VF5	12	1	93	83	101	76-125

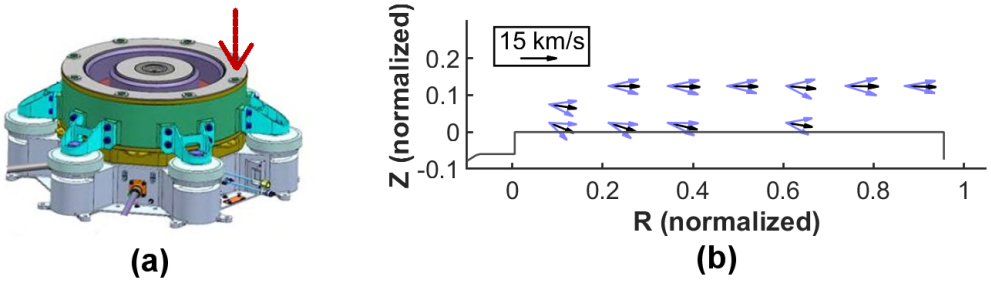

Fig. 3. Example vector plot showing medium-energy ions exiting radially outward from the thruster. Arrow in subplot (a) shows the location of the LIF data relative to the thruster. Subplot (b) shows an example vector plot where the black arrows indicate averaged velocity vector at each data location and blue arrows show the outer boundaries encapsulating 90% of the ions.

Fig. 3 shows a representative example of a vector plot for the LIF data obtained near the outer front pole of the ETU. The arrow in subplot (a) of this figure points to the outer front pole of the ETU, which is the location where the LIF measurements in subplot (b) were taken. In subplot (b), data from the 300 V, 6.3 kW operating condition was plotted. Black arrows indicate averaged velocity vector while blue arrows show the outer boundaries that encapsulate 90% of the ion population at each location.

From the above LIF data, one can see that the TDU and ETU exhibited an independent ion population with averaged energy ranging from 60 to 190 eV, full-width-at-half-maximum energy of 70 to 120 eV, and over angles of 60 to 130 degrees from the firing axis. While the energy varied with various control parameters such as magnetic field strength and background pressure, the angles of travel remain within the aforementioned range. A portion of these ions stop at the outer front pole, causing erosion, while another portion continues out to the surroundings. For the remainder of this paper, these ions will be referred to as side plume ions.

To better understand the trend of the energies of the side plume ions with background pressure, the averaged side plume ion energy near the outer front pole is plotted against background pressure for all pressure studies performed in references [2, 3]. This plot is shown in Fig. 4. In this figure, each plotted point represents the energy averaged over all measurements taken near the outer front pole at that combination of thruster, operating condition, and background pressure. Notably, the averaged energy slightly increased when comparing ions near the outer edge to the inner edge of the outer front pole. For example, if energy was averaged over only the radial outer half of the outer front pole for the 300 V, 2.4 kW condition, the averaged energy is 185 eV as opposed to 175 eV when averaging over the entire outer front pole. Since the ions near the radial outer half are expected to be more representative of the side plume going out to the far-field, the energy of the side plume ions is likely to be slightly higher than what is shown in Table 1 and Fig. 4, but the differences do not affect the trends shown in Fig. 4. Note that the 300-6.3 and 600-12.5 operating conditions correspond to the same discharge current, which is ~20.8 A, whereas the 300-2.4 operating condition correspond to a discharge current of 8 A. Knowing this and then observing Fig. 4, one can see that the discharge voltage appeared to have only a small effect on the ion energy whereas the discharge current has a more pronounced effect. One can hypothesize that the side plume ion energy depends on the local background pressure near the chamfer where the side plume ions are seen to originate (green arrows in Fig. 1). In this scenario, a decrease in global background pressure or a decrease in anode mass flow rate can drive a decrease in local background pressure leading to the side plume ions becoming more energetic.

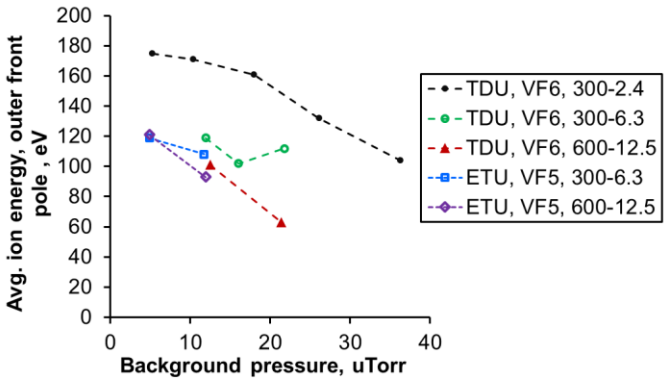

Fig. 4. Averaged ion energy near the outer front pole for TDU and ETU at different background pressures.

From Fig. 4, one can see that the average ion energy of the side plume generally increases with decreasing background pressure. The limited number of data points for some operating condition makes it difficult to determine whether the trend is linear or non-linear. The data suggest that at space-like pressures, the averaged energy of the side plume ions will reach at least 140 eV and can be higher depending on whether the trend becomes non-linear.

Another interesting set of data comes from time-resolved LIF performed near the outer chamfer of the TDU [4]. This data set revealed that for 300 V operations the ion energy distribution was largely constant (up to the ~100 kHz measurement bandwidth) as the discharge current, driven by global oscillation, varied. Whereas for 600 V operations the ion energy distribution varied greatly as the discharge current varied. The difference is driven by whether or not the LIF measurement location is downstream of or periodically inside the acceleration region. For 300 V operation, the data suggest that the environment in which side plume production occurs is on the downstream end of the acceleration region since otherwise we would see large variation in the measured ion energy over time [4-6]. Conversely, for 600 V operation, the data suggest that the environment in which side plume production occurs varies with time as the acceleration zone moves back and forth over the chamfer region, which suggest the possibility that side plume production only occurs over certain phase of the global oscillation action. This idea is explored further in Section IV.

Table 2 summarizes key trends that were deduced from the aforementioned LIF studies performed on the TDU and ETU for the side plume ions. This table lists the controlling parameter, the associated trend, and the references for the test during which the trend was observed.

Table 2. Summary of trends in the side plume characteristics with various control parameters for the TDU and ETU Hall thrusters.

Parameter	Trend description	Reference
Background pressure	**Side plume ions become more energetic with decreasing background pressure.**	[2, 3]
Flow rate (constant voltage)	**Side plume ions become more energetic with decreasing flow rate (decreasing discharge current) at constant voltage.**	[2, 3]
Magnetic field strength	**Side plume ions become more energetic with increasing magnetic field strength.**	[2, 3]
Discharge voltage (constant flow rate)	**Side plume ions exhibited negligible change in energy with varying discharge voltage (constant flow rate).**	[2, 3]
Cathode flow fraction	**Side plume ions exhibited negligible change in energy with varying cathode flow fraction.**	[2]

B. Far-Field Plasma Probe Data

In early plasma plume measurements of the TDU, unexplained ion populations occupying the angular range of 60-100° from the firing axis was found and was thought to be due to charge-exchange actions. While charge-exchange actions are likely to still be involved, LIF data points to the possibility that some of these ions are the same as the side plume ions discovered near the outer front pole.

Fig. 5 subplot (a) and (b) show examples of Faraday probe sweeps performed on the TDU at the 300 V, 6.3 kW and 600 V, 12.5 kW conditions, respectively. This data was collected during TDU long duration wear test [7] and is representative of all TDU and ETU Faraday probe measurements at the same operating conditions. Additional details on the plasma diagnostics can be found in reference [8]. For these measurements, the Faraday probe was swept at five distances, listed in the figure as multiples of the mean channel diameter. Mean channel diameter is the average of the inner and outer diameter of the discharge channel. For each figure, each colored line shows the current density in A/steradian at one distance and the black line shows the current density when linearly extrapolating the data at each angle back to a distance of 0. The black line effective represents what the current density profile looks like prior to being smeared out by collisional effects in the far-field. Details on the extrapolation methodology can be found in reference [9]. In these figures, red arrows point to bumps in the current density corresponding to plasma exiting out the side of the thruster. Also in these figures, one can see that the ion current density (in A/steradian) at the sides of the thruster increases with distance, which implies the currents are being redistributed from the middle to the sides due to collisional effects.

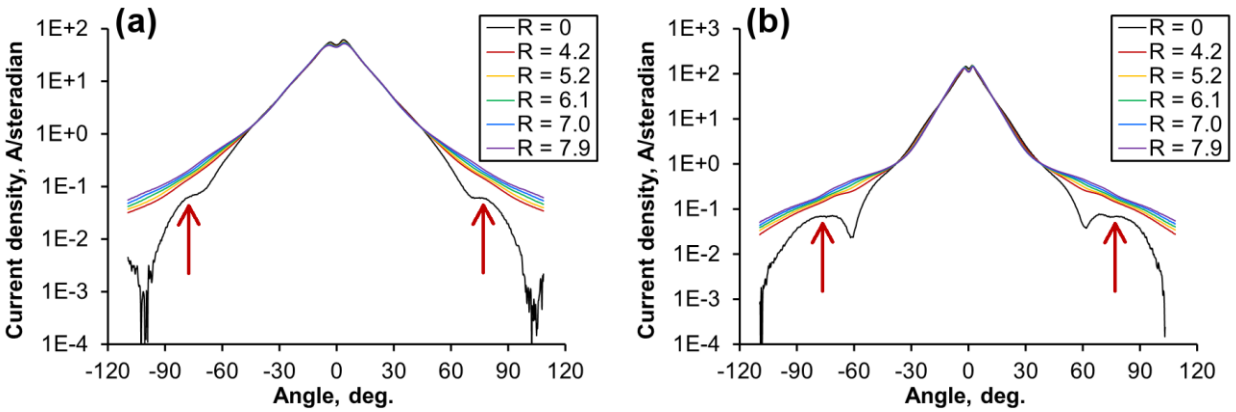

Fig. 5. Faraday probe results showing the presence of ion populations exiting from the sides of the thruster. Subplot (a) shows the TDU results at the 300 V, 6.3 kW condition. Subplot (b) shows the same at the 600 V, 12.5 kW condition.

In addition to current density bumps in the Faraday probe sweeps, RPA measurements also detected ions exiting the side of the TDU and ETU with energies in excess of what is expected from charge exchange actions. Fig. 6 shows an example of ion energy per charge distributions calculated from RPA measurements taken from the ETU2 at the 300 V, 6.3 kW condition, at 80, 90, and 100° from the firing axis. These measurements were made during ETU2 performance characterization [10] and are representative of all TDU and ETU RPA measurements at the same operating condition. The low energy ions seen in the figure is likely from charge-exchange collisions given that their averaged energy is in the 20 to 30 eV range. Independent of the low-energy ions are a group of medium-energy ions occupying the 100 to 200 eV range. At the 80° from firing axis location, one can also observe the presence of beam energy ions independent of the low-energy and medium-energy ions.

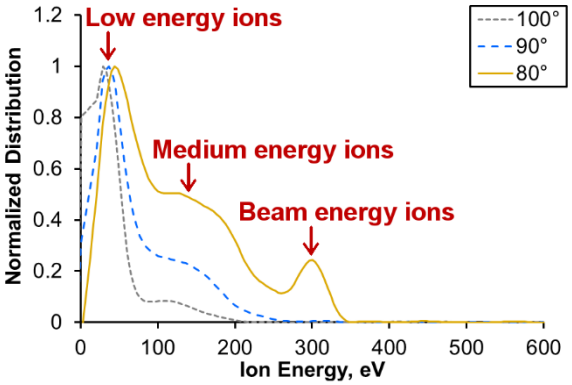

Fig. 6. Far-field Ion energy per charge distribution measured from the ETU2 operating at 300 V, 6.3 kW, at various angles from the firing axis.

Fig. 7 reproduces plots of ion energy per charge distribution versus polar angles for the TDU previously published in reference [8]. Subplots (a) and (b) are for the thruster operating at 300 V, 6.3 kW and 600 V, 12.5 kW, respectively. Pink arrows are added to indicate the location of the side plumes. From this figure, one can observe a sizable increase in ion energy in the far-field RPA data over the angles of 60° to 100° from the firing axis. These ions occupy energies ranging from ~50 to ~200 eV near 75° from the firing axis and drops down to tens of eV at greater than 100° from the firing axis. The observed characteristics are in good agreement with both LIF and Faraday probe data. It is also noteworthy that there appears to be a discrepancy between the exact ion energies seen in the far-field RPA data when compared to that seen in the LIF data, which will be explored in the next section of the paper.

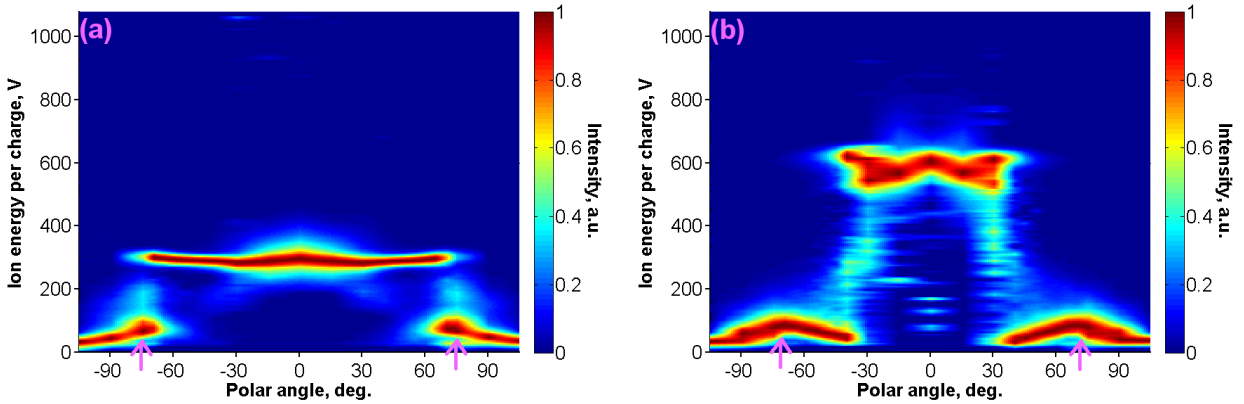

Fig. 7. Plots of ion energy per charge distribution versus polar angle for TDU reproduced from reference [8]. Subplot (a) and (b) shows data from the 300 V, 6.3 kW and 600 V, 12.5 kW conditions, respectively. Pink arrows were added to highlight the location of the side plumes.

C. Formation of Channel Exit Striations

The formation of striation running roughly axially along the exit of ceramic discharge channels of Hall thrusters have been observed going as far back as the SPT-100 [11, 12]. For a review of existing data on channel exit striation, see reference [13]. In particular, Figure 6 of reference [13] contain clear images of striations from the XR-5, PPS-1350, and SPT-100, reproduced from the associated publications. Fig. 8 shows the striations observed on the NASA-103M.XL after a 4,731-hour wear test [14]. In general, striations were found to be spaced roughly 0.2 to 1 mm apart in the azimuthal direction. In particular, a 3-kW laboratory thruster developed striations with spacing of 500-700 μm [15]. Two thrusters, one at >1 kW and one at <1 kW, each developed striations with spacing of ~400 μm [16].

Fig. 8. Striations observed on the outer chamfer of the NASA-103M.XL after 4,731-hour of operations.

No definitive explanation for channel exit striations have been established in the literature but a few hypotheses have been brought up. The fact that the striation spacing is roughly equal to the electron gyro radius in the vicinity of the exit has led to speculations that the striations are related to azimuthal electrostatic waves (a.k.a. spokes) [16] or is at least driven by electron mechanics (such as the Hall current) instead of ion mechanics [17].

While the existence of channel exit striations, by themselves, neither confirm nor deny the existence of the Hall thruster side plume, the existence of striations provides more support for any hypotheses on the origin of the side plume that involves plasma waves than ones that do not. At the very least, the striations provide indirect evidence suggesting that electron waves can exist and can become stationary waves in the region near the channel chamfers where the main beam ions no longer dominate, and magnetic field strength is high. Note that for magnetically shielded thrusters, the term “channel chamfer” refers to a literal, pre-machined chamfer, whereas for non-magnetically shielded thrusters, this term refers to corner on the channel wall at the exit of the channel, which tends to erode into a chamfer over time [11]. No striations have been observed on either the TDU or the ETU as of writing.

III. The Puzzle

While far-field RPA and near-thruster LIF data are in excellent agreement regarding the angular extent of the side plume, there is disagreement in the ion energy observed. Fig. 9 shows a comparison of the ion energy distributions measured by far-field RPA and near-thruster LIF for the ETU operating at 300 V and 6.3 kW. The RPA data were made at several angles from the firing axis while the LIF data is averaged over the radial outer half of the outer front pole. Whereas the RPA measures all charged species present, LIF only measures singly-charged species. From this figure, one can see that a low-energy (few tens eV) population is present in the RPA data that is absent from the LIF

data. When the distribution is normalized, the RPA data is dominated by the low-energy population, which has the tallest peak, while the LIF data consist of a single medium-energy peak.

As previously suggested, the low-energy population is a result of charge-exchange actions where energetic ions exchange charge with slow moving background neutrals and the resulting slow moving ions show up in the far-field. This process also attenuates the number of medium-energy ions showing up in the far-field. For conditions in the TDU and ETU test, charge-exchange mean free path was on the order of a few meters, which was enough to attenuate the number of medium-energy ions by 10-15%, calculated using methodology described in reference [18]. The number of low-energy ions produced by this calculation is far too low to explain the low-energy population seen in the RPA data. One can deduce that most likely the low-energy population in the RPA data come from charge-exchange acting on the main beam ions, which are estimated to be at least three orders of magnitude denser than the medium-energy ions based on the Faraday probe data. From Faraday probe data shown in Fig. 5, one can see that collisions (including charge-exchange) redistributes ions from the main beam near the thruster firing axis out to the sides where the side plume resides. For example, at -90° in Fig. 5(a), current density per steradian in the far-field is ~5 times that of the extrapolated value at R = 0. In comparison, RPA data at -90° in Fig. 9 show a low-energy peak that is ~4 times as voluminous as the medium-energy peak.

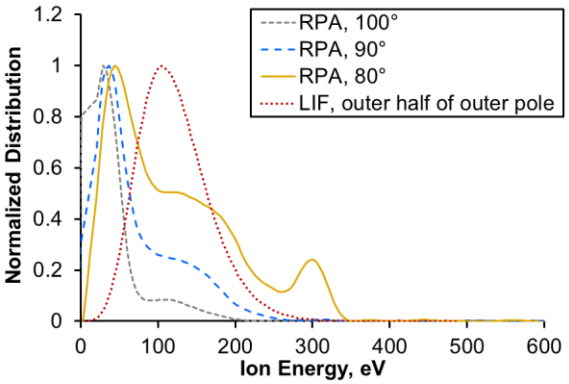

Fig. 9. Ion energy distribution measured by RPA versus LIF for the ETU operating at 300 V, 6.3 kW. RPA data is shown at various angles from firing axis while LIF data is averaged over the radial outer half of the outer front pole.

If the above explanation is correct, one can deduce that at zero background pressure the side plume of magnetically shielded thrusters should have a higher energy than what is measured by far-field RPA in ground test and a lower current density than what is measured by far-field Faraday probe in ground test. Adding in the effect of discharge plasma moving downstream with decreasing background pressure [19, 20] and changes in the mechanism driving the side plume with background pressure (Table 2), the exact trend in the eroding power of the side plume with background pressure is likely to be highly nonlinear.

IV. The Possibilities

A. Ion Heating Driven By Modified Two-Stream Instability

Given the above data, one can study various possible mechanisms for generating the side plume and how well the mechanisms fit the data. The leading hypothesis for the source of the side plume is that it is the same lower hybrid waves believed to be heating the ions that bombard the inner front pole [21, 22]. Of the lower hybrid waves that Mikellides and Lopez Ortega studied [21, 22], the conditions for growth of the modified two-stream instability (MTSI) was established to be favorable in the chamfer region and MTSI will be looked at first.

The key characteristics of MTSI is that it involves a stream of electrons encountering ions with a large relative difference in velocity in the presence of a strong magnetic field [22-24]. The resulting wave specifically propagates in the direction perpendicular to the magnetic field, which for the Hall thruster chamfer region can either be the direction pointing towards and away from the chamfer or the azimuthal direction. The wave transfers energy from the electrons to the ions resulting in heating in the directions perpendicular to the magnetic field. In this phenomenon, the energy reservoir is the electrons that form the Hall current. The amount of energy available scales with the electron temperature. Growth of MTSI is also found to scale with magnetic field strength. Thus, the conditions for MTSI to heat ions exist at the chamfer regions of Hall thruster discharge channel where energetic electrons meet strong magnetic field and ions to be acted on. Fig. 10 illustrates a possible way in which MTSI can generate the observed side plume ions. In this figure, the red circle in each subplot denotes the region where plasma wave activities are believed to be the most intense. Starting from this circled region, if one travels too far radially inward (leftward in the figure), the strength of the magnetic field drops leading to slow wave growth. If one travels too far radially outward (rightward in the figure), the density of electrons and ions drop, possibly leading to the breakup of the wave or energy transfer becoming negligible.

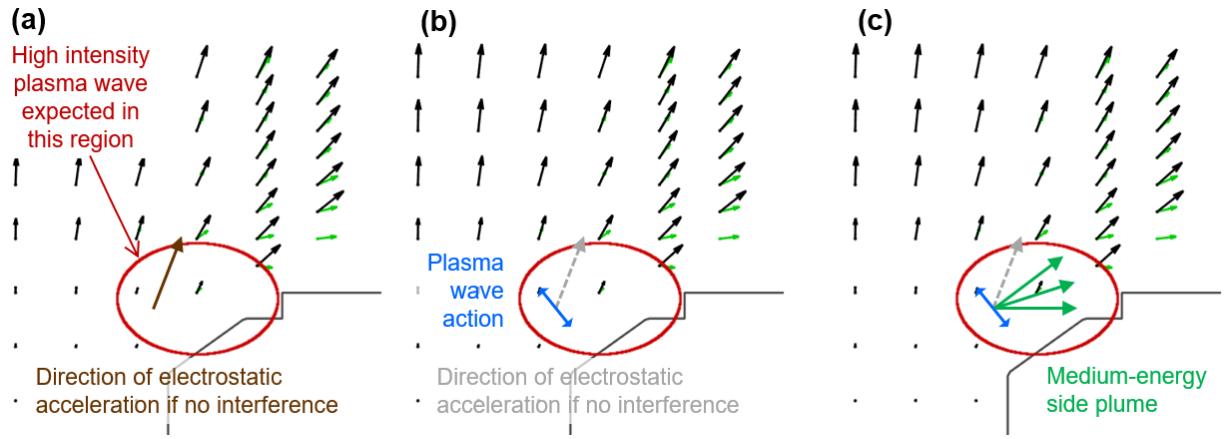

Fig. 10. An illustration of how MTSI can act on the local ions in the outer chamfer region and create a side plume. LIF velocity vector data is used as a background. Brown arrow in subplot (a) shows the trajectory of the local ions in the absence of plasma wave actions. Blue double arrow in subplot (b) shows how the plasma wave action alters the velocity of the local ions. Green arrows in subplot (c) show how the local ions take on new trajectories as a result of plasma wave actions.

In Fig. 10, subplot (a) shows how the local ions in the outer chamfer region start out traveling mostly in the axial direction (up in the figure). Subplot (b) show MTSI acting on the local ions by adding energy to said ions in directions perpendicular to the local magnetic field. Note that the direction of the local magnetic field line and the associated direction of heating varies depending on the exact location and the double arrow drawn is only meant to be illustrative. Also note that heating in the azimuthal direction is also possible though that aspect of heating should have negligible effect on the overall trajectory of the ions when viewed from the thruster far-field. A striking aspect of the heating shown in subplot (b) is that any ions that is energized in the radial inward and downstream direction would quickly leave the area of intense plasma wave action and rejoin the main beam. Whereas any ions that is energized in the radial outward and upstream direction would continue to experience further plasma wave actions by staying near the chamfer. As a result, even though MTSI should cause as many local ions to be deflected inward as outward, the inwardly deflected ions ultimately blend in with the main beam population in the far-field while the outwardly deflected ions experience a prolong period of heating, many of which exit the thruster from the side. This behavior agrees with the far-field Faraday probe (Fig. 5 black line) and RPA data (Fig. 7) where the side plume bumps are very distinct from the main beam population. Note that the mechanism illustrated in Fig. 10 should only work to scatter lower energy ions as higher energy ions (such as accelerated beam ions) will have too much momentum for the plasma wave to effectively turn. The low energy ions that are turned are likely to be ions born locally via impact ionization or charge exchange actions. This would explain why their numbers are very low compared to the main beam.

This paper stated earlier that MTSI can propagate either in-plane (into and away from the chamfer) or in the azimuthal direction. In reality, it is unlikely that any MTSI wave is driven by in-plane propagation due to the very short radial-axial distance over which the magnetic field strength remains high. Instead, propagation of MTSI is very likely to be dominated by azimuthal propagation since in the azimuthal direction the condition for high growth is continuously met. This implies that if MTSI is present, it is very likely to be saturated. The candidate mechanisms that dampen and constrain the growth of MTSI are the availability of energy (from the electrons) and the collisions with neutrals. Given essentially continuous travel for MTSI propagating in the azimuthal direction, even small quantity of neutrals (large mean free path) can affect the level at which MTSI saturates. Furthermore, it is only local neutrals in the chamfer regions that moderates MTSI, implying that not only would the plasma wave actions grow in intensity with decreasing background pressure but would also do so with decreasing anode neutral flow, which matches the behavior observed in the experiments (Table 2 lines 1 and 2). Additionally, collisions with local neutrals moderates the electron temperature of the Hall current. High local neutral density should therefore decrease the amount of free energy available to power MTSI. MTSI is therefore expected to be very sensitive to local neutral density in the chamfer regions.

Given the growth of MTSI scales with magnetic field strength, it is reasonable to infer that MTSI intensity and the resulting side plume will become more energetic with increasing magnetic field strength, which matches experimental observations (Table 2 lines 3). However, it is difficult to determine whether the side plume becomes more energetic as a result of local electron temperature rising with magnetic field strength, or MTSI wave intensity rising with

magnetic field strength, or both. This leaves open the possibility that ion energy of the side plume may scale non-linearly with magnetic field strength.

Given that ion heating driven by MTSI scales with electron temperature, one would expect that the amount of ion heating should increase with discharge voltage as past studies have shown that electron temperature in the discharge channel tends to increase with discharge voltage [25, 26]. Instead, the experimental observation was that the side plume ion energy was largely unaffected by the discharge voltage (Table 2 line 4). It is possible that electron temperature in the outer chamfer region does not vary with discharge voltage the way that electron temperature in the rest of the discharge channel does. Another possibility is that while increasing discharge voltage led to higher electron temperature, it also decreased the amount of plasma entering the region of high MTSI activities, and the two effects cancel out.

Aside from the trend with discharge voltage, there are additional areas of discrepancy between the theory that the side plume is driven by MTSI actions and experimental data. One notable discrepancy is the large difference in the final energies of the ions observed in the side plume and the theoretical maximum energy that MTSI can transfer into the ions (i.e. on the order of the electron temperature). Unless the local electron temperature can reach 150 to 200 eV, it seems unlikely that MTSI action alone can boost side plume ions to the level of energy observed. Furthermore, MTSI actions should produce a spread of ion energies reaching down to tens of eV whereas the LIF measurements show distinct peaks as if resulting from some amount of electrostatic acceleration. One likely source of the electrostatic acceleration is the drop in electric potential between where MTSI is active and the outer front pole as seen in the black arrows in Fig. 1(a). Additionally, electric potential drop, in the range of tens of eV, is seen in the difference in the velocity of the ions found near the inner and outer edges of the outer front pole [2, 3]. However, it is unclear why the side plume ions would increase in energy with increasing magnetic field strength if the majority of the energy comes from electrostatic acceleration or why the spread in the energy distribution would be as wide as observed given kinematic compression effect from electrostatic acceleration. The detailed mechanics of how the chamfer ions can be scattered by MTSI while undergoing electrostatic acceleration need to be studied further.

Another area of disagreement between the MTSI theory and experimental data is that MTSI only heat ions in the direction perpendicular to the magnetic field lines. Although field lines do take on many angles, as a whole they are oriented such that only a small portion of the ion heating occurs in the radial direction. The direction of heating is such that it explains why ions are scattered (Fig. 10), leading to the formation of a precursor ion population that ultimately becomes the side plume, but does not explain how energy from the heating effect become the high radial ion velocities observed.

These aforementioned areas of disagreement leave open the possibility that there are undiscovered aspects to how MTSI behave in the outer chamfer region, other plasma waves at work, or additional mechanisms not related to plasma waves. In particular, Mikellides and Lopez Ortega studied the possibility of the lower hybrid drift instability (LHDI) acting on ions near the inner front pole [22] and this instability may play a role in the energization of the side plume ions.

B. Relation to Channel Exit Striation

As previously mentioned, channel exit striations have been found to have spacing on the order of the electron gyro radius and the presence of azimuthal periodicity strongly implies a standing azimuthal wave. A key characteristic of lower hybrid plasma wave is that the wave number in the direction perpendicular to the magnetic field is tied to the electron. The characteristics of the striations are in agreement with the presence of a lower hybrid plasma wave propagating in the azimuthal direction. While the presence of striation does not imply the presence of MTSI, the presence of striation does provide evidence for the presence of a plasma wave with a wave number that is linked to the properties of the electrons.

Notably, fully shielded Hall thrusters like ETU and TDU, where plasma is fully lifted off of the chamfer, have not exhibited any channel exit striation. One possible explanation is that since the location of plasma wave action is specifically tied to the magnetic field, if the chamfer is moved sufficiently far from the area of action, the amount of erosion will be reduced to below a detectable level. This can come about as a result of plasma density and electron temperature dropping to low enough level that plasma wave actions are no longer supported (i.e. the basic premise of magnetic shielding [27, 28]). Fig. 11 subplot (a) illustrates this explanation. In Fig. 11, black arrows represent the main beam, green arrows represent the side plume, and red dashed circle represent the region of intense plasma wave activities. In contrast to a fully shielded thruster, if a thruster starts with some ceramic channel material in the region of plasma wave action, that material will get worn away by the side plume as illustrated in subplot (b). Eventually, enough of the material is removed such that the side plume barely grazes the remaining surface, and the condition is met for the azimuthal electron wave to become a standing wave, leading to striations. Notable in this theory is that the striations are unlikely to deepen past a certain point as they only started forming after the global rate of erosion dropped

enough for local structures to start forming. The exact mechanism for the deepening of the striation is left for future work.

A final interesting result of this theory is that fully shielded thruster will never develop striation even if the side plume grazes a portion of the chamfer so long as enough of the chamfer becomes coated with conductive material that short circuit the formation of any standing azimuthal electron wave. The azimuthal wave will simply precess azimuthally, and the ions erode the deposited material evenly. It is conceivable that absent a conductive deposit, against an insulating surface, that some level of striation will eventually develop.

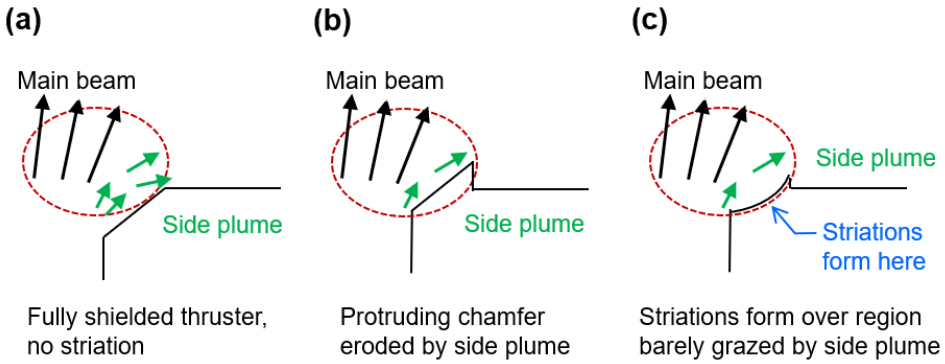

Fig. 11. An illustration of how a fully magnetically shielded Hall thruster may never experience channel exit striations while a thruster with channel materials protruding into the plasma wave action zone will develop striations over time. Subplot (a) illustrates the fully shielded thruster. Subplot (b) illustrates a thruster with channel materials protruding into the plasma wave action zone. Subplot (c) illustrates how the protruding material is worn away by the side plume over time until the side plume barely grazes the remaining surface material and striations develop.

C. Side Plume Driven by Resonant Acceleration

Another possibility for side plume formation is the idea of resonant acceleration. During global discharge oscillations, the acceleration zone tends to move up and downstream in a cyclic manner [4-6, 29, 30]. If MTSI or some similar mechanism only acts during certain parts of this cycle, the resulting ions may take on very specific energies related to where exactly in the cycle they are scattered. For example, it could be that when the global discharge oscillation is at the high density portion of the cycle, more of the plasma enter the plasma wave action zone, where the lower hybrid waves quickly grow and ions are scattered. Since lower hybrid waves have frequencies in the range of MHz to tens of MHz while global oscillations have frequencies of tens of kHz, the lower hybrid waves can quickly grow and saturate when the densest of plasma enters the region of high magnetic field strength. Even if the lower hybrid waves damp out during the portion of global discharge oscillations with low local plasma density, the lower hybrid waves can quickly grow back as soon as the plasma density rises. As a result, the lower hybrid waves may not be active through the entire cycle of global discharge oscillation. If the amount of remaining electric potential drop between the location of the plasma wave action and the far-field is always on the order of 150 to 200 V, then the side plume ions will show up in the far-field with that amount of energy. Notably, the region where plasma wave action is believed to be the most intense also coincide with the downstream portion of the acceleration zone.

The idea of resonant acceleration has some notable flaws. LIF data have shown that the acceleration zone moves upstream with increasing magnetic field strength [2, 3]. This trend implies that at any static location the remaining electric potential compared to the far-field decrease with increasing magnetic field strength. Yet, the ion energy of the side plume increases with increasing magnetic field strength. Similarly, LIF data have shown that the acceleration zone moves upstream with decreasing anode flow rate [2, 3]. Yet, the ion energy of the side plume increases with decreasing anode flow rate.

However, the idea of resonant acceleration should not yet be dismissed because the majority of LIF data from near the outer front pole comes from studying 300 V operations, where it is already known that the plasma condition near the chamfer region does not appear to experience significant variations as the discharge current varies [4]. On the other hand, at the less studied 600 V condition, the plasma condition near the chamfer appear to vary widely. From Fig. 5 (a) of reference [4], one can see that about half of the time the ions present are high energy main beam ions, which would not be susceptible to scattering by MTSI, while the other half of the time the ions present are low in energy and therefore susceptible. There remains the possibility that resonant acceleration only affects some operating conditions and not others.

V. Discussion

While the data gathered provided a basic description of the characteristics of the side plume of two magnetically-shielded Hall thrusters in ground test, it also suggested that the eroding power of this side plume will grow on-orbit when compared to ground test measurements. Not only do facility background neutrals suppress the apparent energy of the side plume ions (as seen in RPA versus LIF data), but the energies of the side plume ions grow with decreasing background pressure (as seen in LIF data versus background pressure). Furthermore, there is a possibility that as the discharge plasma moves downstream with decreasing background pressure [2, 3, 20, 31-33], more ions will be fed into the near-chamfer region leading to higher side plume densities. On the other hand, the current density for the side plume is 3-4 orders of magnitude smaller than the main beam.

One can conclude from the data that this side plume should be factored into future spacecraft integration activities in order to avoid unexpected spacecraft erosion and deposition. At the same time, side plume erosion is not insurmountable and can be accommodated if the designer is aware of its extent. For this reason, it is highly recommended that the community make on-orbit measurements of the side plumes of magnetically shielded Hall thrusters in order to bound the extent of side plume-induced erosion.

Additionally, if the side plume really is produced by plasma wave action and the channel exit striations are linked to said plasma wave, then the possibility exist that all Hall thruster (shielded and non-shielded) have side plumes. The only reason that plasma wave-induced side plume has not been identified sooner is because they have largely been eroding and was blocked by the ceramic walls of older, non-shielded thrusters. The study of this idea is left for future work.

VI. Conclusions

The combination of LIF and plasma probe data collected on two magnetically shielded Hall thrusters have shown that there exist an independent ion population of medium-energy (on average, 60-190 eV) exiting out the side (60° to 100° from firing axis) of the thrusters. Studying the trends with background pressure and known discrepancies between the laser-induced fluorescence and far-field plasma probe data suggest that at zero pressure the side plume is likely to exhibit higher energy and lower density than at facility background pressures.

The possibility that side plume ions were produced by the modified two-stream instability was explored. While a theory based on MTSI fits the existing data very well there are areas of disagreement. In particular, MTSI explains why the side plume ions inevitably takes on a trajectory independent of the main beam ions and show up as distinct bumps in the far-field probe data. MTSI also explains the trend in the side plume ion energy with background pressure, anode mass flow rate, and magnetic field strength. However, MTSI does not provide an immediately obvious explanation for why the side plume ion energy does not vary much with discharge voltage. Further, the measured energy of the side plume ions exceeded the limit of what MTSI can produce by a factor of three or more. If the MTSI-driven theory is correct, the side plume phenomenon is likely to be present in a range of magnetically shielded and non-shielded Hall thrusters.

Based on the idea that channel exit striations may be associated with the same plasma wave phenomenon behind the production of the side plume, a theory for when and how channel exit striations are formed was also proposed. In this theory, channel exit striations are a byproduct of side plume erosion proceeding to the point where the side plume barely grazes the insulating channel wall, setting up the conditions for a standing azimuthal electron wave. The exact mechanism for the deepening of the groove is left for future work.

Lastly, a theory for acceleration of the side plume ions based on these ions only forming during certain phase of the discharge channel global oscillation was explored. In this theory, the side plume ions are only produced with a certain amount of electric potential drop remaining relative to the far-field, leading to the side plume consistently reaching the associated energy in the far-field. Two major areas of disagreement between this theory and experiments as well as a possible explanation for the disagreements were discussed.

Acknowledgments

The authors would like to thank the Space Technology Mission Directorate for funding the Solar Electric Propulsion project and the joint NASA GRC and JPL development of the HERMeS thruster. The authors would like to thank Clayton D. Kachele, George J. Williams, Dean P. Petters, and Timothy D. Smith for managing this electric propulsion work, and David T. Jacobson for technical leadership.

The authors would like to thank Drew M. Ahern, Matthew J. Baird, Gabriel F. Benavides, Maria Choi, Jason D. Frieman, James H. Gilland, Timothy G. Gray, Thomas W. Haag, Daniel A. Herman, Scott J. Hall, Jonathan A. Mackey, James L. Myers, Peter Y. Peterson, Luis R. Pinero, Dale A. Robinson, Timothy R. Sarver-Verhey, and John T. Yim of the NASA Glenn Research Center and Vernon H. Chaplin, Richard R. Hofer, Robert B. Lobbia, Alejandro

Lopez Ortega, Ioannis G. Mikellides, James E. Polk, of the Jet Propulsion Laboratory for work on the SEP HERMeS and AEPS Hall thruster system. The authors would like to thank Kevin L. Blake, Matthew T. Daugherty, Joshua D. Gibson, Larry F. Hambley, Michael A. Harkleroad, Chad E. Joppeck, Nick Lalli, John M. Lauerhahs, Michael McVetta, Derek Patterson, Richard Polak, Kevin J. Rahill, Thomas A. Ralys, Richard G. Senyitko, Luke Sorrelle, and James M. Szelagowski for assembly of the test setup as well as operation of the vacuum facilities.

References

[1] Huang, W., Kamhawi, H., and Herman, D. A., "Ion Velocity in the Discharge Channel and Near-Field of the HERMeS Hall Thruster", *2018 Joint Propulsion Conference*, AIAA-2018-4723, Cincinnati, OH, Jul 9-11, 2018. https://doi.org/10.2514/6.2018-4723

[2] Huang, W., Frieman, J. D., Kamhawi, H., Peterson, P. Y., and Hofer, R. R., "Ion Velocity Characterization of the 12.5-kW Advanced Electric Propulsion System Engineering Hall Thruster", *2021 AIAA Propulsion and Energy Forum*, AIAA-2021-3432, Virtual, Aug 9-11, 2021. https://doi.org/10.2514/6.2021-3432

[3] Huang, W. and Kamhawi, H., "Counterstreaming ions at the inner pole of a magnetically shielded Hall thruster", *Journal of Applied Physics*, Vol. 129, Jan 27, 2021, pp. 043305. https://doi.org/10.1063/5.0029428

[4] Chaplin, V. H., Lobbia, R. B., Lopez Ortega, A., Mikellides, I. G., Hofer, R. R., Polk, J. E., and Friss, A. J., "Time-resolved ion velocity measurements in a high-power Hall thruster using laser-induced fluorescence with transfer function averaging", *Applied Physics Letters*, Vol. 116, No. 23, Jun 11, 2020, pp. 234107. https://doi.org/10.1063/5.0007161

[5] Chaplin, V. H., Jorns, B. A., Conversano, R. W., Lobbia, R. B., Lopez Ortega, A., Mikellides, I. G., and Hofer, R. R., "Laser Induced Fluorescence Measurements of the Acceleration Zone in the 12.5 kW HERMeS Hall Thruster", *35th International Electric Propulsion Conference*, 2017-229, Atlanta, GA, Oct 8-12, 2017.

[6] Durot, C. J., Georgin, M. P., and Gallimore, A. D., "Time-Resolved Laser-Induced Fluorescence Measurements in the Plume of a 6-kW Hall Thruster", *34th International Electric Propulsion Conference*, 2015-399, Kobe, Japan, Jul 4-10, 2015.

[7] Frieman, J. D., Kamhawi, H., Mackey, J. A., Haag, T. W., Peterson, P. Y., Herman, D. A., Gilland, J. H., and Hofer, R. R., "Completion of the Long Duration Wear Test of the NASA HERMeS Hall Thruster", *2019 AIAA Propulsion and Energy Forum*, AIAA-2019-3895, Indianapolis, IN, Aug 19-22, 2019. https://doi.org/10.2514/6.2019-3895

[8] Huang, W., Williams, G. J., Peterson, P. Y., Kamhawi, H., Gilland, J. H., and Herman, D. A., "Plasma Plume Characterization of the HERMeS during a 1722-hr Wear Test Campaign", *35th International Electric Propulsion Conference*, 2017-307, Atlanta, GA, Oct 8-12, 2017.

[9] Huang, W., Kamhawi, H., Haag, T. W., Lopez Ortega, A., and Mikellides, I. G., "Facility Effect Characterization Test of NASA's HERMeS Hall Thruster", *52nd AIAA/SAE/ASEE Joint Propulsion Conference*, AIAA-2016-4828, Salt Lake City, UT, Jul 25-27, 2016. https://doi.org/10.2514/6.2016-4828

[10] Frieman, J. D., Kamhawi, H., Huang, W., Mackey, J. A., Ahern, D. M., Peterson, P. Y., Gilland, J. H., Hall, S. J., Hofer, R. R., Branch, N. A., Dao, H., Inaba, D., and Welander, B., "Performance of the 12.5-kW Advanced Electric Propulsion System Engineering Test Unit Hall Thruster", *68th Joint Army-Navy-NASA-Air Force Propulsion Meeting*, Virtual, Jun 7-17, 2021.

[11] Arhipov, B. A., Bober, A. S., Gnizdor, R. Y., Kozubsky, K. N., Korakin, A. I., Maslennikov, N. A., and Pridannikov, S. Y., "The Results of 7000-Hour SPT-100 Life Testing", *24th International Electric Propulsion Conference*, 1995-039, Moscow, Russia, Sep, 1995.

[12] Garner, C. E., Brophy, J. R., Polk, J. E., and Pless, L. C., "A 5,730-Hr Cyclic Endurance Test of the SPT-100", *31st AIAA/ASME/SAE/ASEE Joint Propulsion Conference*, AIAA-1995-2667, Pasadena, CA, Jul 10-12, 1995. https://doi.org/10.2514/6.1995-2667

[13] Brown, N. P. and Walker, M. L., "Review of Plasma-Induced Hall Thruster Erosion", *Applied Sciences*, Vol. 2020, No. 10:3775, May, 2020. https://doi.org/10.3390/app10113775

[14] Kamhawi, H., Manzella, D. H., Pinero, L. R., Haag, T. W., and Huang, W., "In-Space Propulsion High Voltage Hall Accelerator Development Project Overview", *46th AIAA/ASME/SAE/ASEE Joint Propulsion Conference & Exhibit*, AIAA-2010-6860, Nashville, TN, Jul 25-28, 2010. https://doi.org/10.2514/6.2010-6860

[15] Abashkin, V. V., Gorshkov, O. A., Lovtsov, A. S., and Shagaida, A. A., "Analysis of Ceramic Erosion Characteristic in Hall-Effect Thruster with Higher Specific Impulse", *30th International Electric Propulsion Conference*, 2007-133, Florence, Italy, Sep 17-20, 2007.

[16] Zidar, D. G. and Rovey, J. L., "Hall-Effect Thruster Channel Surface Properties Investigation", *Journal of Propulsion and Power*, Vol. 28, No. 2, Mar-Apr, 2012, pp. 334-343. https://doi.org/10.2514/1.B34312

[17] Mazouffre, S., Dubois, F., Albarede, L., Pagnon, D., Touzeau, M., and Dudeck, M., "Plasma induced erosion phenomena in a Hall thruster", *International Conference on Recent Advances in Space Technologies*, Istanbul, Turkey, Nov 20-22, 2003. https://doi.org/10.1109/RAST.2003.1303393

[18] Shastry, R., Hofer, R. R., Reid, B. M., and Gallimore, A. D., "Method for analyzing ExB probe spectra from Hall thruster plumes", *Review of Scientific Instruments*, Vol. 80, No. 6, Jun 22, 2009, pp. 063502. https://doi.org/10.1063/1.3152218

[19] Huang, W., Kamhawi, H., and Peterson, P. Y., "Effects of Background Pressure and Electrical Configuration on the Velocity Field of the HERMeS Hall Thruster", *2020 AIAA Propulsion and Energy Forum*, AIAA-2020-3616, Virtual, Aug 24-28, 2020. https://doi.org/10.2514/6.2020-3616

[20] Cusson, S. E., Dale, E. T., Jorns, B. A., and Gallimore, A. D., "Acceleration region dynamics in a magnetically shielded Hall thruster", *Physics of Plasmas*, Vol. 26, No. 2, Feb 5, 2019, pp. 023506. https://doi.org/10.1063/1.5079414

[21] Mikellides, I. G. and Lopez Ortega, A., "Growth of the modified two-stream instability in the plume of a magnetically shielded Hall thruster", *Physics of Plasmas*, Vol. 27, No. 10, Oct 5, 2020, pp. 100701. https://doi.org/10.1063/5.0020075

[22] Mikellides, I. G. and Lopez Ortega, A., "Growth of the lower hybrid drift instability in the plume of a magnetically shielded Hall thruster", *Journal of Applied Physics*, Vol. 129, No. 19, May 17, 2021, pp. 193301. https://doi.org/10.1063/5.0048706

[23] McBride, J. B., Ott, E., Boris, J. P., and Orens, J. H., "Theory and Simulation of Turbulent Heating by the Modified Two-Stream Instability", *The Physics of Fluids*, Vol. 15, No. 12, Mar, 1972, pp. 2367-2383. https://doi.org/10.1063/1.1693881

[24] Ott, E., McBride, J. B., Orens, J. H., and Boris, J. P., "Turbulent Heating in Computer Simulations of the Modified Plasma Two-Stream Instability", *Physical Review Letters*, Vol. 28, No. 2, Jan, 1972, pp. 88. https://doi.org/10.1103/PhysRevLett.28.88

[25] Shastry, R., Huang, W., Haag, T. W., and Kamhawi, H., "Langmuir Probe Measurements within the Discharge Channel of the 20-kW NASA-300M and NASA-300MS Hall Thrusters", *33rd International Electric Propulsion Conference*, 2013-122, Washington, DC, Oct 6-10, 2013.

[26] Herman, D. A., Shastry, R., Huang, W., Soulas, G. C., and Kamhawi, H., "Plasma Potential and Langmuir Probe Measurements in the Near-field Plume of the NASA 300M Hall Thruster", *48th AIAA/ASME/SAE/ASEE Joint Propulsion Conference & Exhibit*, AIAA-2012-4115, Atlanta, GA, Jul 29-Aug 1, 2012. https://doi.org/10.2514/6.2012-4115

[27] Mikellides, I. G., Katz, I., Hofer, R. R., and Goebel, D. M., "Magnetic shielding of a laboratory Hall thruster. I. Theory and validation", *Journal of Applied Physics*, Vol. 115, No. 4, Jan 24, 2014, pp. 043303. https://doi.org/10.1063/1.4862313

[28] Hofer, R. R., Goebel, D. M., Mikellides, I. G., and Katz, I., "Magnetic shielding of a laboratory Hall thruster. II. Experiments", *Journal of Applied Physics*, Vol. 115, No. 4, Jan 24, 2014, pp. 043304. https://doi.org/10.1063/1.4862314

[29] Fife, J. M., Martinez-Sanchez, M., and Szabo, J., "A Numerical Study of Low-Frequency Discharge Oscillations in Hall Thrusters", *33rd AIAA/ASME/SAE/ASEE Joint Propulsion Conference*, AIAA-1997-3052, Seattle, WA, Jul 6-9, 1997. https://doi.org/10.2514/6.1997-3052

[30] Lobbia, R. B., "A Time-resolved Investigation of the Hall Thruster Breathing Mode", Ph.D. Dissertation, Aerospace Engineering, University of Michigan, Ann Arbor, MI, 2009.

[31] Nakles, M. R. and Hargus, W. A., Jr., "Background Pressure Effects on Ion Velocity Distribution Within a Medium-Power Hall Thruster", *Journal of Propulsion and Power*, Vol. 27, No. 4, Jul-Aug, 2011, pp. 737-743. https://doi.org/10.2514/1.48027

[32] Mazouffre, S., "Laser-induced fluorescence diagnostics of the cross-field discharge of Hall thrusters", *Plasma Sources Science and Technology*, Vol. 22, No. 1, Nov 29, 2012, pp. 013001. https://doi.org/10.1088/0963-0252/22/1/013001

[33] MacDonald-Tenenbaum, N., Pratt, Q., Nakles, M. R., Pilgram, N., Holmes, M., and Hargus, W. A., Jr., "Background Pressure Effects on Ion Velocity Distributions in an SPT-100 Hall Thruster", *Journal of Propulsion and Power*, Vol. 35, No. 2, Mar-Apr, 2019, pp. 403-412. https://doi.org/10.2514/1.B37133